Change in Neuronal Firing Patterns in the Process of Motor Command Generation for the Ocular Following Response

AYA TAKEMURA,[1,2] YUKA INOUE,[1] HIROAKI GOMI,[2,3] MITSUO KAWATO,[4] AND KENJI KAWANO[1,2]
[1]*Neuroscience Research Institute, Electrotechnical Laboratory, National Institute of Advanced Industrial Science and Technology;* [2]*Core Research for Evolutional Science and Technology, Japan Science and Technology, Ibaraki 305-8568;* [3]*NTT Communication Science Laboratories, Nippon Telegraph and Telephone Corporation, Kanagawa 243-0198; and* [4]*Advanced Telecommunications Research Institute International, Kyoto 619-0288, Japan*

Received 16 April 2001; accepted in final form 5 July 2001

Takemura, Aya, Yuka Inoue, Hiroaki Gomi, Mitsuo Kawato, and Kenji Kawano. Change in neuronal firing patterns in the process of motor command generation for the ocular following response. *J Neurophysiol* 86: 1750–1763, 2001. To explore the process of motor command generation for the ocular following response, we recorded the activity of single neurons in the medial superior temporal (MST) area of the cortex, the dorsolateral pontine nucleus (DLPN), and the ventral paraflocculus (VPFL) of the cerebellum of alert monkeys during ocular following elicited by sudden movements of a large-field pattern. Using second-order linear-regression models, we analyzed the quantitative relationships between neuronal firing frequency patterns and eye movements or retinal errors specified by three parameters (position, velocity, and acceleration). We first attempted to reconstruct the temporal waveform of each neuronal response to each visual stimulus and computed the coefficients for each parameter using the least-square error method for each stimulus condition. The temporal firing patterns were generally well reconstructed [coefficient of determination index (CD) $>$ 0.7] from either the retinal error or the associated ocular following response. In the MST and DLPN datasets, however, the fit with the retinal error model was generally better than with the eye-movement model, and the estimated coefficients of acceleration and velocity ranged widely, indicating that temporal patterns in these regions showed considerable diversity. The acceleration component is greater in MST and DLPN than in VPFL, suggesting that an integration occurs in this pathway. When we determined how well the temporal patterns of the neuronal responses of a given cell could be reconstructed for all visual stimuli using a single set of coefficients, good fits were found only for Purkinje cells (P-cells) in the VPFL using the eye-movement model. In these cases, the coefficients of acceleration and velocity for each cell were similar, and the mean ratio of the acceleration and velocity coefficients was close to that of motor neurons. These results indicate that individual MST and DLPN neurons are each encoding some selective aspects of the sensory stimulus (visual motion), whereas the P-cells in VPFL are encoding the complete dynamic command signals for the associated motor response (ocular following). We conclude that the sensory-to-motor transformation for the ocular following response occurs at the P-cells in VPFL.

INTRODUCTION

Ocular following responses are slow tracking eye movements evoked by sudden drifting movements of a large-field visual stimulus in primates. These responses help to stabilize the eyes on the visual scene. Experiments using monkeys have revealed many features of ocular following (Kawano and Miles 1986; Miles and Kawano 1986; Miles et al. 1986). One of the most interesting features of ocular following is that it has an observed latency of as short as 50 ms. Considering the delays introduced in the retina and the ocular motor plant, the intervening neural elements must be limited in sequential number, suggesting that this system may be amenable to characterization at all stages, from sensory input to motor output.

Previous studies have found that neurons in the medial superior temporal (MST) area of the cortex (Kawano et al. 1994), the dorsolateral pontine nucleus (DLPN) (Kawano et al. 1992), and the ventral paraflocculus (VPFL) of the cerebellum (Shidara and Kawano 1993) of the monkey respond with directional selectivity to movements of a large-field visual stimulus. In most cases, their firing rate begins to increase before the eye movement.

The MST sends strong projections to the DLPN (Brodal 1978; Glickstein et al. 1980, 1985; Maunsell and van Essen 1983; May and Andersen 1986; Ungerleider et al. 1984), and the DLPN sends projections to the cerebellum, mainly to the flocculus (paraflocculus) and lobules VI and VII of the vermis (Brodal 1979, 1982; Langer et al. 1985). Recent anatomical studies have shown that the DLPN sends only a light projection to the flocculus. In contrast, DLPN projections to the VPFL and dorsal paraflocculus are substantial (Glickstein et al. 1994; Nagao et al. 1997). Furthermore, lesion studies of the MST (Shidara et al. 1991; Takemura et al. 2000), DLPN (Kawano et al. 1990) and VPFL (unpublished observations) have shown that injection of suppressive chemicals into any of these regions produces a decrement in ipsilateral ocular following responses. Evidence from these single-unit recordings and focal chemical lesions have suggested that early ocular following responses are mediated by a pathway that includes the MST, DLPN, and VPFL.

To understand what the temporal pattern of a Purkinje cell (P-cell) in the VPFL represents, Shidara et al. (1993) and Gomi et al. (1998) used a linear time-series regression analysis. They showed that the simple spike activities of the P-cells during ocular following could be reconstructed by an inverse-dynamics representation. This successful reconstruction suggested that the firing frequencies of the P-cells represent the dynamic

Address for reprint requests: A. Takemura, Neuroscience Research Institute, AIST, 1-1-1, Umezono, Tsukuba, Ibaraki 305-8568, Japan (E-mail: a.takemura@aist.go.jp).

 0022-3077/01 $5.00 Copyright © 2001 The American Physiological Society

motor command used by downstream structures to elicit ocular following. However, the transformation of visual information into motor commands for eye movement has yet to be characterized.

To examine how the motor command is generated in the information-processing stream, we analyzed the temporal patterns of single units in the neural circuit for ocular following, specifically, the MST, DLPN, and VPFL. The purposes of this study are to understand what the temporal neuronal activities in the MST and DLPN represent and to understand the difference among the MST, DLPN, and VPFL.

To investigate the information represented in the discharges of MST and DLPN neurons and of P-cells in the VPFL from the viewpoint of motor command generation, we applied a second-order linear-regression model (the inverse-dynamics representation) using eye movement to reconstruct the temporal firing patterns. Conversely, to examine the neural discharges from the viewpoint of visual signal transformation, we used retinal error instead of eye movement in the model. Furthermore, to investigate the relationship between the firing patterns and retinal error/eye movement under a single condition or multiple conditions, we used local and global fitting, respectively. In the analyses, we focus on the differences between the fitting performances in global/local fittings from sensory/motor signals and the estimated coefficients representing characteristics of the neural discharges. Our results indicate that the information represented in the firing patterns of MST and DLPN neurons were similar to each other, but differed from those of P-cells in the VPFL. Based on our observations, we provide a hypothetical scheme of spatiotemporal and sensory-to-motor transformations for ocular following. Preliminary results from these analyses have been presented elsewhere (Takemura et al. 1996, 1999).

METHODS

Data were collected from nine adolescent Japanese monkeys (*Macaca Fuscata*), weighting 5–9 kg. All animals had been trained previously to fixate on a small target spot on a tangent screen for a liquid reward (Wurtz 1969). A cylinder for chronic recording of single neuron activity was implanted under aseptic conditions into each monkey under pentobarbital sodium anesthesia. A fixture was attached that allowed the head to be fixed in the standard stereotaxic position during the experiments. Scleral search coils were implanted into both eyes to record eye movements according to the technique of Judge et al. (1980). Eye position was monitored by an electromagnetic induction technique (Fuchs and Robinson 1966). The coil output voltages were calibrated for eye position by having the animal fixate on small light-emitting diode (LED) targets at known positions along the horizontal and vertical meridians. All experimental protocols were approved by the Electrotechnical Laboratory Animal Care and Use Committee.

Behavioral paradigms and visual stimuli

The behavioral paradigms and visual stimuli used in this study were identical to those of Shidara and Kawano (1993) and are described elsewhere (Kawano et al. 1992, 1994; Shidara and Kawano 1993). In brief, during the recording sessions, the monkey sat in a primate chair with its head secured to the chair facing a translucent screen (85 × 85°) located 235 or 500 mm in front of the animal. The visual stimulus was back-projected onto the screen as a ramp movement of a random-dot pattern. Each ramp started 50 ms (in some cases, 100–300 ms) after the end of a saccade directed toward the central part of the screen. The stimulus lasted 250–300 ms, then the screen went blank for 0.5–2 s while the animal remained in the dark. The ramps were presented at five speeds (10, 20, 40, 80, and 160°/s) and in eight directions (right, left, up, down, and the 4 diagonal directions). The monkeys were given an occasional drop of fruit juice to help them remain alert and to facilitate fast saccades.

Recording technique

Single-unit activities were recorded using tungsten microelectrodes implanted in the MST, DLPN, or VPFL. A hydraulic microdrive (Narishige Mo-9) was mounted on the recording cylinder, and glass-coated tungsten microelectrodes were used to initially identify and map each region and its neighboring structures. A fixed grid system (Crist et al. 1988) was then used to introduce and fix in place a stainless steel guide tube through the dura. The tips of the guide tubes were positioned 3–5 mm above the MST, DLPN, or VPFL. Flexible tungsten electrodes were used to record through the tube.

Acquisition of behavioral and unit data

Our previous studies indicated that neurons in the MST and DLPN and P-cells in the VPFL discharge during brief, sudden movements of a large-field visual stimulus that elicits ocular following (Kawano et al. 1992, 1994; Shidara and Kawano 1993). Most of these neurons increase their firing rate before the eye movements begin. To further characterize the response properties of neurons involved in sensory-to-motor information processing for ocular following, we first selected neurons according to their discharge sensitivity to a moving visual scene that elicited ocular following. After isolating a single unit, we observed its responses to a visual scene moving at 80°/s in eight directions. We selected neurons in which the activity was modulated by one of these stimuli (the preferred direction). We then moved the visual scene in the preferred direction and recorded the neuronal and ocular responses at five different speeds.

During the ocular following response, the mirror velocity and the horizontal and vertical components of eye position and velocity (measured with the search coils and filtered with a 6-pole analog Bessel filter using a cutoff frequency of 100 Hz), were recorded at 500 Hz. The speed of the random-dot pattern on the screen was proportional to the mirror velocity. The single-cell activity of each region was isolated using a time-amplitude window discriminator and was simultaneously recorded at 1,000 Hz. Some of the data presented here were taken from prior studies (Kawano et al. 1992, 1994; Shidara and Kawano 1993) and were reanalyzed.

Data preparation

We selected neurons whose responses to each stimulus were recorded for more than 30 trials under each condition. The firing frequency of each neuron and the eye movement during 30 trials under the same stimulus conditions were ensemble averaged for each cell after excluding trials with saccadic intrusion (35 MST neurons, 32 DLPN neurons, and 20 P-cells). The responses were aligned with the stimulus onset (*time 0*), and the eye acceleration profiles were obtained by digital differentiation of eye-velocity profiles after averaging. Retinal errors as a visual motion signal were obtained by subtracting eye movements from mirror movements. To align the filtering delays, the ensemble average firing pattern (i.e., the firing frequency temporal pattern) was low-pass filtered with a 6-pole Bessel digital filter using the same cutoff frequency (100 Hz) as that of the analog filter for the eye movements. For reasons that we shall go into later, all data were low-pass filtered with the same cutoff frequency to avoid an estimation error (the Butterworth filter cutoff was 50 Hz).

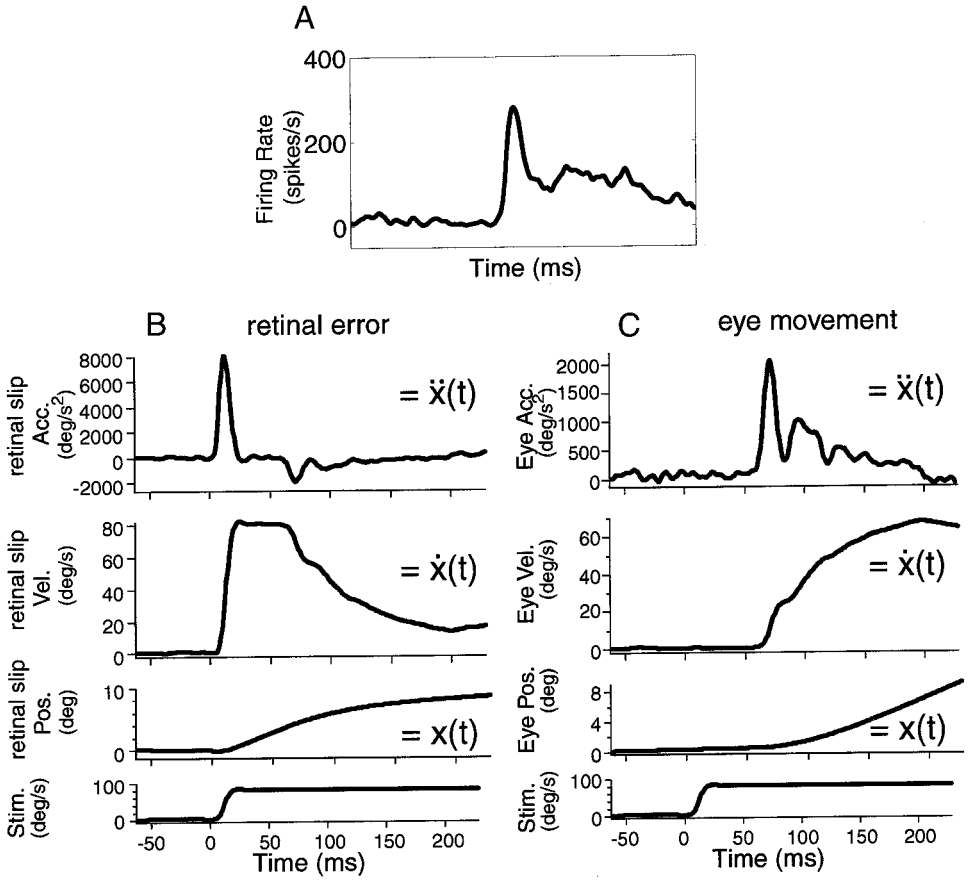

FIG. 1. The ensemble averaged patterns of 40 trials under the same stimulus conditions (preferred direction stimulus, downward ramps at 80°/s). The temporal patterns are aligned with the stimulus onset. *A*: the firing frequency of a single medial superior temporal area (MST) neuron. *B*: temporal patterns of retinal errors. From *top* to *bottom*: the ensemble averaged vertical retinal error acceleration, velocity, and position, and the average stimulus velocity profiles. An upward deflection in the figure indicates a downward retinal error or stimulus movement. *C*: temporal patterns of the ocular following responses. From *top* to *bottom*: the ensemble averaged vertical eye acceleration, velocity, and position, and the average stimulus velocity profiles. An upward deflection in the figure indicates a downward eye or stimulus movement. All data were filtered with a Butterworth low-pass filter (cutoff, 50 Hz). ACC, acceleration; VEL, velocity; POS, position; STIM, stimulus velocity.

Analysis method (linear-regression models of firing rate)

To quantitatively analyze the relationship between sensory/motor information and neural activity, we used a linear time-series regression method (Gomi et al. 1998; Shidara et al. 1993). We applied the same linear-regression model to the neuronal activity of each region using acceleration, velocity, and position of sensory or motor information (retinal errors shown in Fig. 1*B*; eye movements shown in Fig. 1*C*). Figure 1 shows the temporal patterns of each retinal error component as input and eye movements as output, with the temporal pattern of an MST neuron. The equation used for the analysis is as follows

$$\hat{f}(t-\delta) = a \cdot \ddot{x}(t) + b \cdot \dot{x}(t) + c \cdot x(t) + d \qquad (1)$$

where $\hat{f}(t)$, $\ddot{x}(t)$, $\dot{x}(t)$, $x(t)$, and δ are the reconstructed firing frequency of a neuron; the acceleration, velocity, and position of eye movement or retinal error at time t and the time delay, respectively (Fig. 1). Four coefficients (a, b, c, and d) and the time delay (δ) were estimated in such a way as to minimize the squared estimation error. To estimate each coefficient at a particular δ, a linear-regression method was applied to the firing pattern from 10 ms after stimulus onset (ramp onset) to 2 ms before the end of the stimulus (the duration was 238 or 288 ms). The search range for δ was limited from -20 to 20 ms for the eye movement components, and from -80 to -30 ms for the retinal error components.

The coefficient of determination index (CD) (Gomi et al. 1998; Hines and Montgomery 1972) expressed in the *Eq. 2* was used to evaluate the performance of the model

$$\mathrm{CD} = 1 - \sum_t (\hat{f}(t) - f(t))^2 / \sum_t (f(t) - \bar{f})^2 \qquad (2)$$

where $\hat{f}(t)$, $f(t)$, and $\bar{f}$ indicate the reconstructed firing frequency, the observed firing frequency at time t, and the averaged firing frequency during the observation period, respectively. The CD ranges from 0 to 1. As the CD approaches 1, the reconstructed firing frequency is near the observed value, which equals the square of the correlation coefficient. If the CD is close to 1, it suggests that the temporal patterns of the firing frequency encode the temporal patterns of visual motion or motor command. If the firing frequencies are not linearly correlated with the acceleration, velocity, or position of the eye movements or retinal errors, the index approaches zero. The CD depends on the variance of the observed firing frequency (i.e., the signal-to-noise ratio). Because the variations in firing probabilities differ among the three regions, we applied a low-pass filter (the Butterworth filter) to cut frequency components (>50 Hz) that were higher than the dominant components of the retinal errors and eye movements. Consequently, we could avoid any noise contamination in comparing the characteristics of the firing patterns in different brain regions.

Local and global fitting

Previous studies demonstrated that the magnitude of ocular following is strongly dependent on stimulus speed (Miles et al. 1986). Recent experiments also demonstrated that different temporal patterns of firing frequency could be induced by different stimulus speeds. That is, neural responses are also strongly dependent on stimulus speed (Kawano et al. 1992, 1994; Shidara and Kawano 1993). To investigate the relationship between firing pattern and sensory/motor information under the single-stimulus condition, we used local fitting (Gomi et al. 1998). By applying the model to the firing pattern at one of the five speeds, a local relationship between the neuronal firing pattern and retinal errors or ocular responses can be examined. The temporal firing patterns in response to the five stimulus speeds in the preferred direction of a neuron were reconstructed by each set of parameters. This yielded five sets of parameters calculated per neuron. On the other hand, we used global fitting to test whether the model

could be applied independently of stimulus speed such that all five responses could be reconstructed together using a single set of parameters from retinal errors or eye movements (Gomi et al. 1998). To investigate the characteristics of the neural activities, we focused on the reliable parameters using the Student's *t*-test, in which the *P* values of the *t*-test indicate the probability of the null hypothesis (that the coefficient of each component is 0). The model's applicability was evaluated by Cp statistics. The technical details and results are described in the APPENDIX.

RESULTS

We successfully recorded the activities of single units in the MST, DLPN, and VPFL, all of which represent different stages of the information-processing stream, from sensory input to motor output for ocular following. To investigate the relationship between neuronal activity and retinal errors or eye movements under single (local fitting) or multiple (global fitting) stimulus conditions, we used *Eq. 1* to quantitatively analyze temporal firing patterns during ocular following responses in the preferred directions.

Fitting performances of the retinal error model

The traces in Fig. 2, *A* and *B*, summarize the results of reconstructing the firing patterns of an MST neuron from retinal errors under local (*A*) and global fitting (*B*). In Fig. 2, *A* and *B*, each pair of traces shows the firing patterns aligned with the onset of the ramp motion. Within each pair, the thick trace (labeled "reconstruction") shows the reconstructed firing patterns from retinal acceleration, velocity, and position under local (Fig. 2*A*) and global fitting (Fig. 2*B*). The thin trace (labeled "observed data") in each pair shows the observed firing pattern, which is based on the same data at the same stimulus speed as in Fig. 2, *A* and *B*. As shown in Fig. 2*A* (local fitting), all reconstructed firing patterns were very close to the observed data within each pair. Their CDs were between 0.82 and 0.94 (mean value, 0.85), indicating extremely good reconstruction at each of the five stimulus speeds. Under local fitting, the linear-regression model for retinal errors was applicable to most of the data from the MST [shaded area of Fig. 2*C*; CD $\geq$ 0.7 (131/175, 75%)]. On the other hand, as shown in Fig. 2*B* (global fitting), the reconstructed firing patterns were quite different from the observed data in each of the pairs. The calculated CD was 0.35, indicating a failed reconstruction of the five temporal patterns from retinal errors using a single set of parameters. The CDs for a large percentage of MST neurons (88%, 27/35) were lower than 0.7 (blank area of Fig. 2*D*) under global fitting, indicating that the firing patterns of most MST neurons were not adequately reconstructed from retinal errors using only a single set of parameters.

The results obtained from DLPN neurons were similar to those obtained from MST neurons. Most of the data from the DLPN (71%, 114/160) were satisfactorily reconstructed by the retinal error model under local fitting (CD $\geq$ 0.7). Under global fitting, however, the CDs for a large percentage of DLPN neurons (75%, 24/32) were $<$0.7.

Figure 3 summarizes the results of reconstructing the firing patterns of a P-cell from retinal errors under local (*A*) and global fitting (*B*). As shown in Fig. 3*A* (local fitting), all reconstructed firing patterns were close to the observed data within each pair. The CDs were between 0.72 and 0.96 (mean value, 0.87), indicating a good reconstruction at each of the five stimulus speeds. Most of the data from P-cells (89%, 89/100) were satisfactorily reconstructed from retinal errors under local fitting (CD $\geq$ 0.7, in shaded area of Fig. 3*C*). On the other hand, as shown in Fig. 3*B* (global fitting), the reconstructed firing patterns were quite different from the observed data in each of the pairs. The CD was 0.68, indicating a failed reconstruction of the five temporal patterns from retinal errors using a single set of parameters. Global fitting was accurate only for a small percentage of the VPFL P-cells [CD $\geq$ 0.7 (7/20, 35%), in the shaded area of Fig. 3*D*].

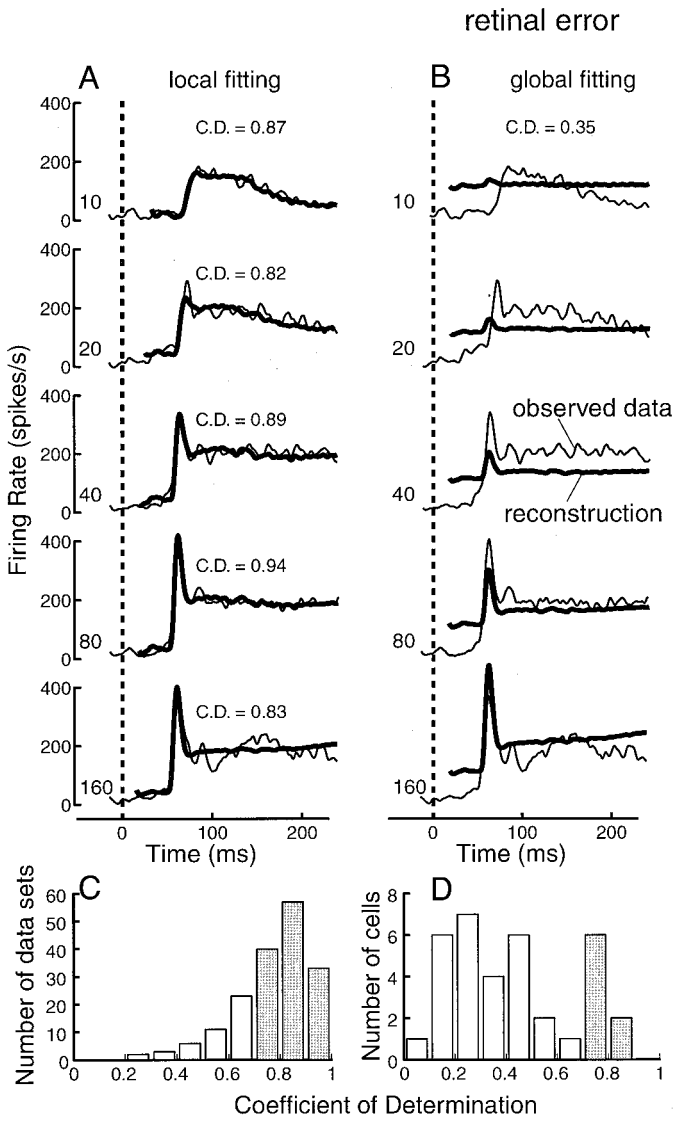

FIG. 2. Reconstruction of the temporal firing patterns of an MST neuron at 5 stimulus velocities from retinal errors. *A*: the model was applied separately to the firing pattern at each of the 5 stimulus speeds (local fitting). *B*: the model was applied to firing patterns at all 5 stimulus speeds with a single set of parameters (global fitting). The stimulus speed is indicated by the numbers to the *left* of the traces. The traces show the observed firing frequency profiles (thin line) and the firing frequency profiles reconstructed from retinal errors (thick line). Traces are aligned with the beginning of the ramps (time = 0 ms). *C* and *D*: frequency histograms of the coefficient of determination indexes (CDs) for 175 MST neuron datasets for local fitting (*C*) and for 35 MST neurons for global fitting (*D*). ▨: CD $\geq$ 0.7.

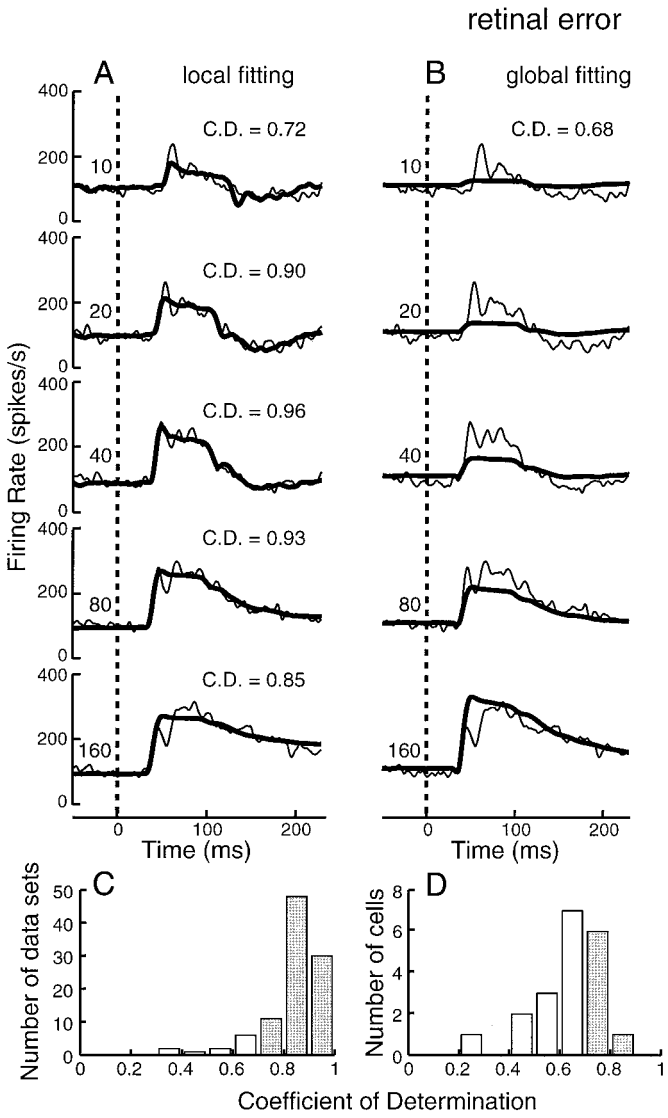

FIG. 3. Reconstruction of the firing patterns of a P-cell at 5 stimulus velocities from retinal errors. *A*: local fitting. *B*: global fitting. The stimulus speed is indicated by the numbers to the *left* of the traces. Traces are aligned with the beginning of the ramps (time = 0 ms). *C* and *D*: frequency histograms of the CDs for 100 P-cell datasets (*C*) and for 20 P-cells (*D*). ▨, CD ≥ 0.7.

From the preceding analyses, the following features common to MST, DLPN, and VPFL neurons were evident. The firing patterns of most neurons were successfully reconstructed by local fitting. However, reconstruction was unsatisfactory using retinal error during global fitting.

Estimated parameters of the retinal error model

To investigate the information represented in the temporal firing patterns, we focused on the reliable coefficients of acceleration, velocity, and position of retinal errors under local fitting. After applying a threshold (≥0.7) to the CDs of the local fittings, we performed a statistical analysis in which the significance of each coefficient was examined by the *t*-test for the null hypothesis (that the coefficient of each component is 0). The number of datasets that fell under a particular *t*-test *P* value is shown in Table 1*A*. In most datasets from MST and DLPN neurons (67.2%, 88/131 and 76.3%, 87/114, respectively), the null hypothesis for the acceleration component was rejected. On the other hand, in only one-fifth of the datasets from VPFL P-cells (21.3%, 19/89), the null hypothesis for the acceleration component was rejected. These results indicate that the necessity for the acceleration component to be presented in P-cell firing patterns is less than that for the MST and DLPN neuronal firing patterns. Meanwhile, the small *P* value for the other components (i.e., velocity, positional, and bias components) indicates that these components are necessary for adequate reconstruction in all regions.

The *t*-test analysis suggests that the information on retinal errors represented in the temporal firing patterns of the MST and DLPN neurons is similar but differs from that of P-cells. To characterize the temporal firing patterns of the three regions, we investigated reliably estimated parameters (coefficient of acceleration, velocity, and position). We first examined whether the distributions of the estimated coefficients were different in the three regions. Figure 4 shows the relationships between the acceleration and velocity parameters, which were both reliably estimated (CD ≥ 0.7 and $P < 0.05$) by the retinal error model under local fitting. As shown in Fig. 4, the MST and DLPN neurons (represented by □ and △, respectively) were more widely scattered than P-cells (represented by ●). There

TABLE 1. *Summary of the t-test P values*

	No. of Datasets		
	$P < 0.005$	$0.005 < P < 0.05$	$0.05 < P$
A. Local fitting by the retinal error model			
MST			
Acceleration component	84 (64.1)	4 (3.1)	43 (32.8)
Velocity component	131 (100)	0 (0.0)	0 (0.0)
Positional component	107 (81.7)	12 (9.2)	12 (9.2)
DLPN			
Acceleration component	87 (76.3)	0 (0.0)	27 (23.7)
Velocity component	114 (100)	0 (0.0)	0 (0.0)
Positional component	91 (79.8)	5 (4.4)	18 (15.8)
VPFL			
Acceleration component	18 (20.2)	1 (1.1)	70 (78.7)
Velocity component	89 (100)	0 (0.0)	0 (0.0)
Positional component	72 (80.9)	2 (2.2)	15 (16.9)
B. Local fitting by the eye-movement model			
MST			
Acceleration component	92 (92.9)	0 (0.0)	7 (7.1)
Velocity component	97 (98.0)	0 (0.0)	2 (2.0)
Positional component	81 (81.8)	3 (3.0)	15 (15.2)
DLPN			
Acceleration component	66 (97.7)	0 (0.0)	2 (2.3)
Velocity component	79 (89.8)	1 (1.1)	8 (9.1)
Positional component	69 (78.4)	8 (9.1)	11 (12.5)
VPFL			
Acceleration component	78 (94.0)	0 (0.0)	5 (6.0)
Velocity component	83 (100)	0 (0.0)	0 (0.0)
Positional component	77 (92.8)	2 (2.4)	4 (4.8)

Summary table of the *t*-test *P* values, showing the significance probability of the null hypothesis (that the coefficient of each component is 0). Percentages are in parentheses. *A*: the *P* values obtained for the medial superior temporal area (MST), dorsolateral pantine nucleus (DLPN), and ventral paraflocculus of the cerebellum (VPFL) by applying the retinal error model. *B*: the *P* values obtained for the MST, DLPN, and VPFL by applying the eye-movement model. If the *P* value is small, the model fitting is poor when that component is dropped.

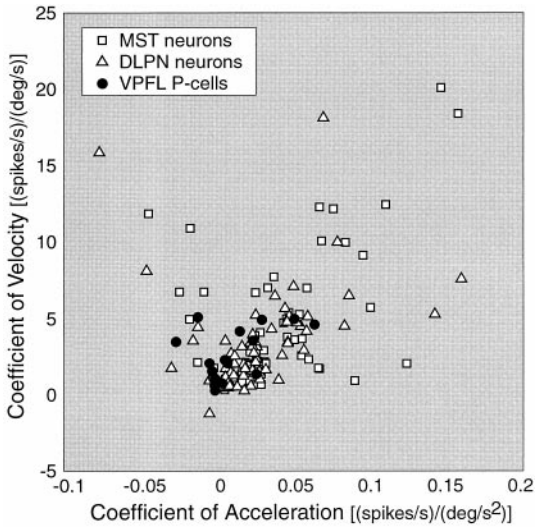

FIG. 4. A comparison of the distributions of the estimated coefficients (abscissa, acceleration coefficient; ordinate, velocity coefficients) by the retinal error model under local fitting. Each point indicates the reliable estimated parameters (CD ≥ 0.7 and $P < 0.05$) of a dataset at a given stimulus speed for a given neuron. MST neurons (□), dorsolateral pontine nucleus (DLPN), neurons (△), and ventral paraflocculus (VPFL) of the cerebellum (VPFL) P-cells (●).

were various cell types (acceleration- or velocity-dominant cells) in the MST and DLPN. Their temporal pattern characteristics were very different from each other. The means of the acceleration coefficients for the MST and DLPN neurons and the VPFL P-cell datasets were 0.032 ± 0.036, 0.025 ± 0.034, and 0.009 ± 0.022 (spikes/s)/(°/s^2), respectively. The magnitudes of the acceleration coefficients of the MST and DLPN neurons were approximately threefold greater than those of the VPFL P-cells. Furthermore, differences in the distributions of the acceleration coefficients were significant at the $P < 0.0015$ level between the MST and VPFL and at the $P < 0.01$ level between the DLPN and VPFL, respectively (by Wilcoxon's rank-sum test). The difference in the distributions of the acceleration coefficients between the MST and DLPN, however, was not significant ($P = 0.24$).

The means of the velocity coefficients for the MST and DLPN neurons and the VPFL P-cell datasets were 3.81 ± 4.04, 3.24 ± 3.18, and 2.50 ± 1.69 (spikes/s)/(°/s), respectively. The magnitudes of the velocity coefficients in the firing patterns of the MST and DLPN neurons and P-cells were similar. The differences in their distributions were not significant ($P = 0.71$ for the MST vs. DLPN, $P = 0.59$ for the DLPN vs. VPFL, and $P = 0.41$ for the MST vs. VPFL, by Wilcoxon's rank-sum test).

The means of the position coefficients were 5.61 ± 13.54 (spikes/s)/° for the MST neuron datasets, -8.06 ± 35.38 (spikes/s)/° for the DLPN neuron datasets, and 7.16 ± 27.19 (spikes/s)/° for the VPFL P-cell datasets. The distribution of the DLPN positional components was significantly different from that of the MST and VPFL ($P < 0.00005$ for the MST vs. DLPN, $P < 0.05$ for the DLPN vs. VPFL, and $P = 0.85$ for the MST vs. VPFL, by Wilcoxon's rank-sum test).

We next examined whether the relationship between the stimulus speed and the goodness of fit (CD) under local fitting differed among the three regions. However, we will first review the directional and speed sensitivities of the MST and DLPN neurons and the P-cells. The neurons analyzed in this study were direction-selective. Therefore their neuronal responses increased for stimuli moving in their optimal direction. To understand the temporal neuronal activities in MST and DLPN neurons and P-cells, we studied their temporal firing patterns using stimuli moving in their optimal direction at 10–160°/s. There were also speed-selective neurons, as shown in Figs. 2 and 3. The temporal firing patterns of these neurons were of different magnitudes, depending on stimulus speed.

To determine the optimal speed for each neuron, we measured the magnitudes of the neuronal responses over the time period analyzed by the linear-regression method. Some MST neurons (13/35, 37%) showed their best response at high stimulus speed (160°/s), whereas others (19/35, 54%) showed their best response at a moderate stimulus speed (40 and 80°/s). Most of the DLPN neurons (25/32, 78%) and P-cells (15/20, 75%) showed their best responses at high stimulus speed (160°/s). Significant differences were observed between the speed preferences for the MST and DLPN/VPFL ($P < 0.002$ for the MST vs. DLPN and MST vs. VPFL, by Wilcoxon's rank-sum test). However, no significant difference was observed between the speed preferences of the DLPN and VPFL ($P = 0.94$).

Because we were interested in the relationship between the optimal speed and fitting performance, we first normalized the stimulus speed to the optimal speed [$\log_2$ (stimulus speed/optimal speed)]. Figure 5 shows the average CD as a function of the normalized stimulus speed for 35 MST neurons (*A*), 32 DLPN neurons (*B*), and 20 P-cells (*C*). As shown in Fig. 5*A*, the fitting performance (CD) of the MST was significantly reduced as the stimulus speed moved away from the preferred speed regardless of whether it was faster or slower. On the

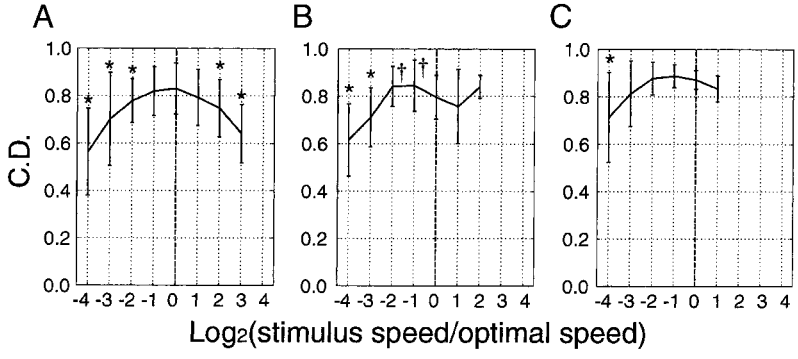

FIG. 5. The relationship between fitting performance (CD) and optimal speed for neurons in the MST (*A*), DLPN (*B*), and VPFL (*C*). The normalized stimulus speed (the abscissa) is plotted on a logarithmic scale [$\log_2$ (stimulus speed/optimal speed)]. The ordinate axis represents the average CD obtained from the retinal error model under local fitting. *, the fitting performance was significantly reduced ($P < 0.05$); †, the fitting performance was significantly increased ($P < 0.05$).

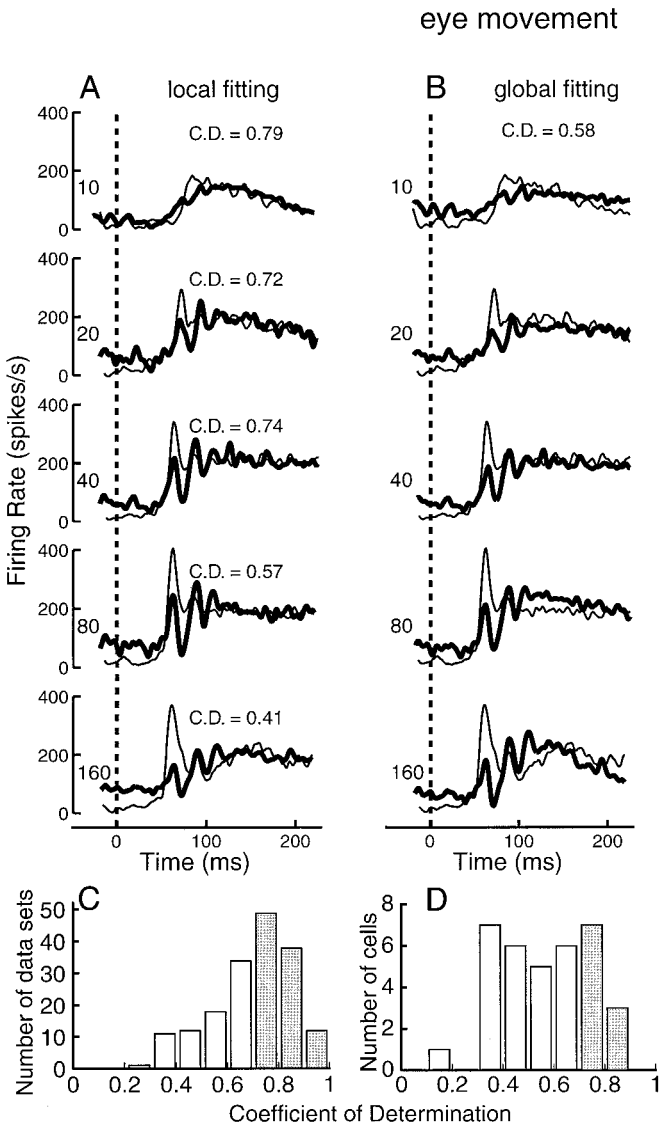

FIG. 6. Reconstruction from eye movements of the firing patterns of the same MST neuron as in Fig. 2 at 5 stimulus velocities. *A*: local fitting. *B*: global fitting. The stimulus speed is indicated by the numbers to the *left* of the traces. Traces are aligned with the beginning of ramps (time = 0 ms). *C* and *D*: freqency histograms of the CDs for 175 MST neuron datasets (*C*) and for 35 MST neurons (*D*). ▨, CD ≥ 0.7.

other hand, the fitting performance of the DLPN and VPFL was not significantly reduced over the range −2 to +2 (Fig. 5, *B* and *C*). These results indicate that the temporal firing patterns of MST neurons represented information on retinal errors only near their optimal speed.

Fitting performances of the eye-movement model

Figure 6 summarizes the fitting performances of the eye-movement model under local (*A*) and global (*B*) fitting for the same MST neurons that were used in Fig. 2. As shown in Fig. 6*A*, the CDs were between 0.41 and 0.79 (mean value, 0.65), indicating that the firing patterns at lower stimulus speeds were relatively well reconstructed. In Fig. 6*B*, the traces in each pair show that the MST firing patterns were not adequately reconstructed under global fitting. The CD was 0.58, indicating a nonlinear relationship between MST firing and ocular responses through multiple stimulus speeds. Under local fitting (Fig. 6*C*, ▨), 57% of the data from the MST (99/175) were reconstructed relatively well from eye movements. Under global fitting, however, the reconstructed firing patterns were not able to approximate the observed firing patterns of most MST neurons (71%, 25/35; Fig. 6*D*, □).

The results obtained from DLPN neurons were similar to those obtained from MST neurons. Under local fitting, 55% of the data from the DLPN (88/160) was reconstructed relatively well from eye movements, whereas global fitting produced a CD of ≥0.7 in a small percentage of the DLPN neurons (31%, 10/32). It is clear from these results that the eye-movement model accounted for the different neuronal responses of only a small portion of neurons in the MST and DLPN under multiple stimulus speeds and using a single set of parameters.

On the other hand, the traces in Fig. 7 summarize the results of reconstructing the firing patterns of the same P-cell as in Fig.

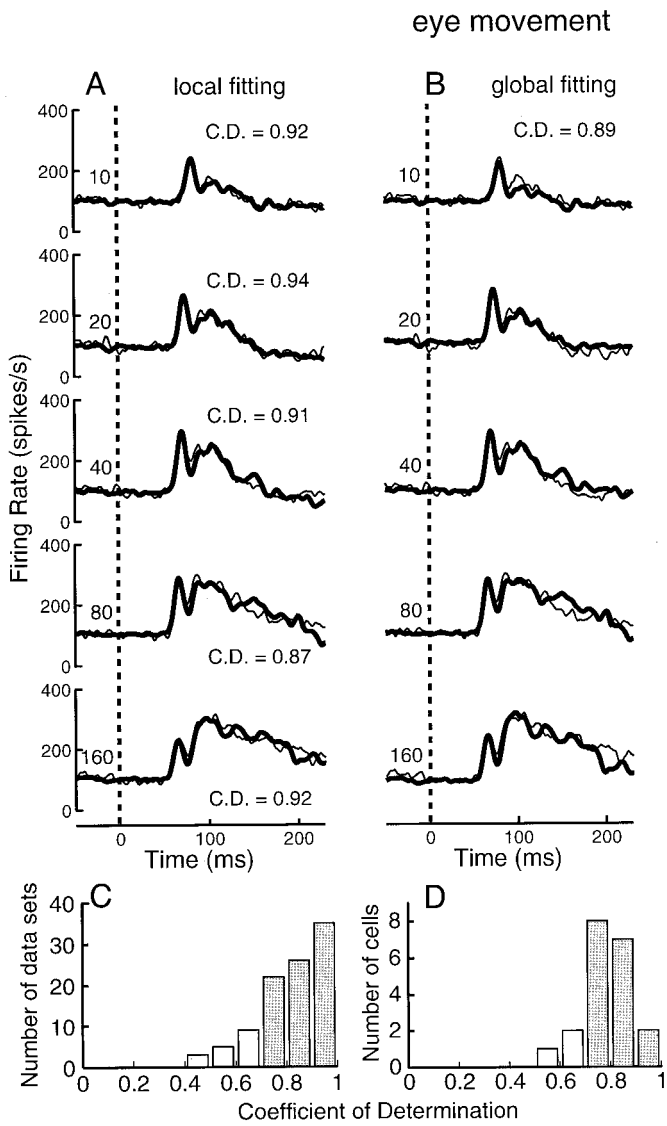

FIG. 7. Reconstruction from eye movements of the firing patterns of the same P-cell as in Fig. 3 at 5 stimulus velocities. *A*: local fitting. *B*: global fitting. The stimulus speed is indicated by the numbers to the *left* of the traces. Traces are aligned with the beginning of ramps (time = 0 ms). *C* and *D*: frequency histograms of the CDs for 100 P-cell datasets (*C*) and for 20 P-cells (*D*). ▨, CD ≥ 0.7.

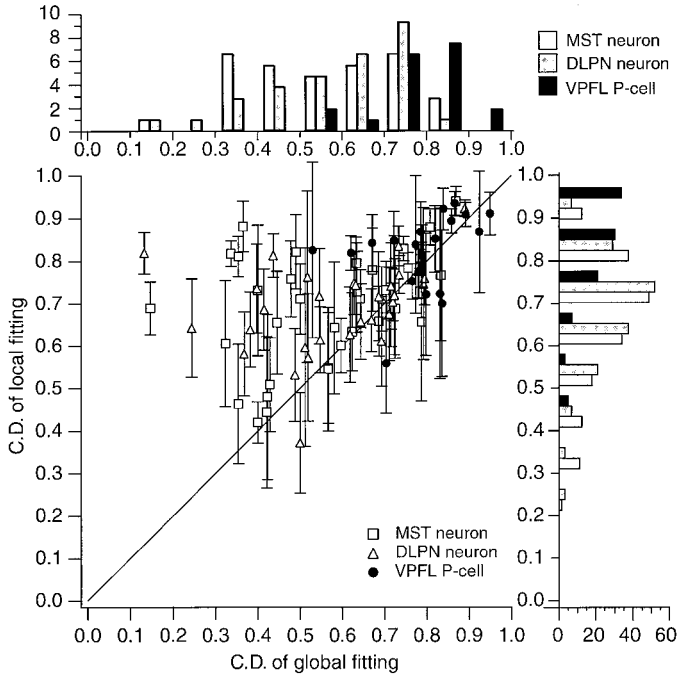

FIG. 8. Summary of the reconstruction of firing patterns by the eye-movement model under local and global fitting. Each point indicates one of the MST neurons (□), DLPN neurons (△), or VPFL P-cells (●). The CDs of global fitting are plotted on the abscissa, and CDs of local fitting are plotted on the ordinate. For global fitting, 1 CD was calculated for each neuron. For local fitting, since the model was applied separately at each of the 5 speeds, 5 CDs were calculated for each neuron; the means ± SD are plotted. *Top*: frequency histogram of the CDs for 35 MST neurons (□), 32 DLPN neurons (▨), and 20 VPFL neurons (■) under global fitting. *Right*: frequency histogram of the CDs for datasets from 175 MST neurons (□), 160 DLPN neurons (▨), and 100 VPFL neurons (■) under local fitting.

3 from eye movements under local (*A*) and global fitting (*B*) at five different speeds. In Fig. 7*A*, the reconstructed firing patterns under local fitting were very close to the observed data within each pair. The CDs were between 0.87 and 0.94 (mean value, 0.91), indicating good reconstruction at each of the five stimulus speeds. In addition, in Fig. 7*B*, the reconstructed firing patterns under global fitting were also very close to the observed data in all pairs. The CD was 0.89, again indicating good reconstruction at each of the five stimulus speeds using only a single set of parameters. These results indicate a linear relationship between P-cell firing and ocular responses at multiple stimulus speeds. The linear-regression model (*Eq. 1*) for eye movement was inapplicable in only a small number of P-cell firing patterns under both local and global fitting (Fig. 7, *C* and *D*, □, 15/100 and 3/20, respectively; CD < 0.7).[1]

As illustrated in Fig. 8, comparing the fitting performances of temporal firing patterns from eye movements for the MST and DLPN neurons and for the VPFL P-cells revealed distinct differences. In this figure, the CDs are displayed for global fitting (the abscissa) and for local fitting (the ordinate). The fitting performances of the VPFL P-cells (●) are distributed in the right top quadrant of Fig. 8, indicating that the temporal firing patterns of the P-cells were satisfactorily reconstructed from eye movement components using the linear-regression model for both local and global fitting [CD ≥ 0.7 in 85/100 datasets of the VPFL (85.0%) in local fitting; CD ≥ 0.7 in 17/20 P-cells (85%) in global fitting]. On the other hand, fitting performances of the DLPN (△) and MST neurons (□) were distributed above the slope line 1. This indicates that we were able to attain a relatively good fit under local fitting [CD ≥ 0.7 in 99/175 datasets of the MST (56.6%) and 88/160 datasets of the DLPN (55.0%)]. When we used global fitting for the MST and DLPN neurons, however, the model adequately reproduced the firing patterns for only a small number of neurons [CD ≥ 0.8 in 3/35 MST (8.6%) and 1/32 DLPN neurons (3.1%); CD ≥ 0.7 in 11/35 MST (33.3%) and 10/32 DLPN neurons (31.3%)]. On the other hand, as demonstrated in the preceding text, global fitting was accurate for most of the P-cells [CD ≥ 0.8 in 9/20 (45%); CD ≥ 0.7 in 17/20 P-cells (85%)]. In Fig. 8, frequency histograms of the CDs for the MST, DLPN, and VPFL datasets under both local and global fitting clearly show the similar tendencies of the MST and DLPN. Figure 8 also reveals the difference between the VPFL and upstream structures (the MST and DLPN).

From the preceding analyses, the following differences between MST and DLPN neurons and P-cells were evident: the temporal firing patterns of the MST and DLPN neurons were successfully reconstructed under local fitting for one-half of the neurons but for only one-third of the neurons under global fitting, but the temporal firing patterns of the P-cells were satisfactorily reconstructed from eye movements under both local and global fitting.

Estimated parameters of the eye-movement model

After applying a threshold ($\geq$0.7) to the CDs of local fittings, we performed the *t*-test analysis. In local fitting, the number of datasets that could be classified under a particular *t*-test *P* value is listed in Table 1*B*. The null hypothesis for the eye acceleration component was rejected ($0.005 > P$) in most datasets from all three regions [92.9% (92/99) for the MST, 97.7% (86/88) for the DLPN, and 94.0% (78/83) for the VPFL]. The *P* values for the other components (i.e., eye velocity and positional components) were also small, and the null hypothesis for these components was rejected ($P < 0.05$). This indicates that all of the components in *Eq. 1* make a significant contribution to describing the relationship between temporal firing patterns and eye movements. We investigated the estimated coefficients for the datasets at different speeds. Figure 9 shows the relationship between the acceleration and velocity parameters, which were both reliably estimated (CD ≥ 0.7 and $P < 0.05$) by the eye-movement model under local fitting. As shown in this figure, the MST data (Fig. 9*A*, □) and the DLPN data (Fig. 9*B*, △) are more widely scattered than the VPFL data (Fig. 9*C*, ●). Each symbol represents the coefficients of acceleration and velocity of a neuron at the slowest stimulus. These parameters for a neuron at different stimulus speeds are connected (—); the lines in Fig. 9, *A* and *B*, extend further than those in Fig. 9*C*.

There are three implications of the data presented in Fig. 9. First, the magnitudes of the acceleration and velocity coefficients varied at different speeds and in different cells, espe-

[1] In this paper, we focus only on the neuronal responses to the preferred directions because the MST and DLPN neurons showed little response (neither an increase nor a decrease in firing rate) to nonpreferred directions. In addition, we used the low-pass filter to compare the temporal firing patterns of different regions (see METHODS). These differences in methods between previous studies (Gomi et al. 1998; Kitama et al. 1999; Shidara et al. 1993) and our study resulted in a high CD for P-cells in this paper, under both local and global fitting using eye movement.

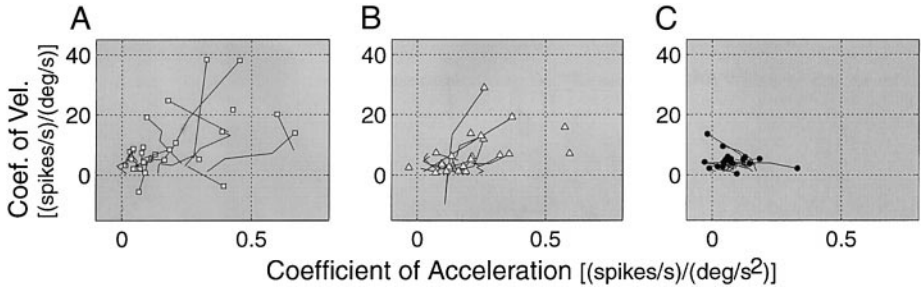

FIG. 9. Comparison of the relationships between acceleration (abscissa) and velocity coefficients (ordinate) estimated by the eye-movement model under local fitting. Each line merges the reliable estimated parameters (CD $\geq$ 0.7 and $P <$ 0.05) for each neuron under different speed conditions; MST neurons (*A*, □), DLPN neurons (*B*, △), and VPFL P-cells (*C*, ●); the data points marked by these symbols are for the slowest stimulus.

cially in the MST and DLPN (Fig. 9, *A* and *B*). Second, the magnitudes of the velocity coefficients for slow stimuli were frequently larger than those for fast stimuli (the *y* axis in Fig. 9), especially in the MST and DLPN. Third, the magnitudes of the acceleration coefficients for slow stimuli were often larger than those for fast stimuli in the DLPN (the *x* axis in Fig. 9).

In summary, the firing frequencies of the MST and DLPN neurons were reconstructed successfully for one-half of the datasets by the eye-movement model under local fitting. In MST and DLPN neurons, the coefficients for different cells and for different stimulus speeds within a cell were different and widely scattered. On the other hand, the firing frequencies of the VPFL P-cells were reconstructed successfully for most datasets, and their coefficients were similar to each other.

As was the case with local fitting, the results of global fitting also demonstrated that the temporal firing patterns in the MST and DLPN were different from those in the VPFL. We examined the reliability of estimated parameters that had a high CD ($>$0.7) by the eye-movement model under global fitting. The significance of each coefficient was $<$0.02 in all units, except one P-cell (11/11 MST neurons, 10/10 DLPN neurons, and 16/17 P-cells).

The mean lead-time of the neuronal response with respect to the onset of eye movement was 11.8 $\pm$ 3.6 (SD) ms for MST neurons and 11.9 $\pm$ 6.9 ms for DLPN neurons. These values agree with those of previous studies on the relative latency to the onset of the stimulus of MST neural activity (Kawano et al. 1994) and DLPN neural activity (Kawano et al. 1992) during ocular following. The mean time delay of VPFL P-cells was 7.7 $\pm$ 5.1 ms, which is near the latency period for electrical-stimulation-evoked eye movements (Shidara and Kawano 1993).

To compare the component data obtained from MST and DLPN neurons and P-cells with corresponding data from motor neurons (Keller 1973), we calculated the ratios of the acceleration, velocity, and position coefficients (Table 2). The mean ratios of the acceleration coefficient to the velocity coefficient (b/a) of MST (36.5) and DLPN neurons (24.7) differed from those of motor neurons (67.4). This was because the acceleration coefficient tended to be larger than that of the motor neurons. On the other hand, as reported previously (Gomi et al. 1998; Shidara et al. 1993), the mean ratio of the acceleration coefficient to the velocity coefficient (b/a) of P-cells (50.1) was close to that of motor neurons (67.4). Thus the acceleration coefficient of MST and DLPN neurons tended to be larger than that of the P-cells. Meanwhile, the mean ratio of the acceleration coefficient to the position coefficient (c/a) differed between the MST, DLPN, and VPFL, and was of negative sign.

TABLE 2. *Ratios of the coefficients (b/a) in each of the three regions and in motor neurons*

	Acceleration: Velocity: Position
MST neurons	1:36.5:−190.7
DLPN neurons	1:24.7:−34.7
Purkinje cells	1:50.1:−236.7
Motor neurons (from Keller's data)	1:67.4:344.8

Comparison of the performances in local and global fittings from retinal error and from eye movement

The boxes in Fig. 10 summarize the fitting performance (i.e., the CD values) of all regression analyses (*left*, local and global

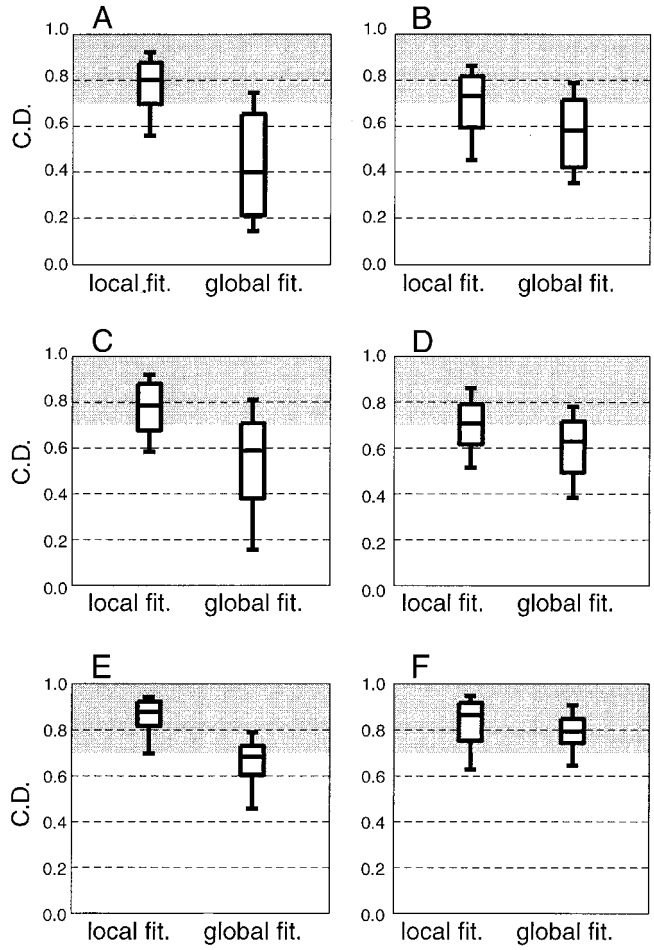

FIG. 10. Summary of the linear-regression analysis for MST, DLPN, and VPFL cells from retinal errors (*A*, *C*, and *E*) or eye movements (*B*, *D*, and *F*) under local or global fitting. *Top* to *bottom*: distribution of CDs in the MST, DLPN, and VPFL. Left/right box-plot in each panel: under local/global fitting. Each box-plot shows the 10, 25, 50, 75, and 90th distribution percentiles.

fitting by the retinal error model; *right*, eye-movement model). In the retinal error model (*left*), the differences between the distributions of CDs under local and global fitting were significant ($P < 0.0001$) in all three regions (the Mann-Whitney U tests of nonparametric tests). This indicates that neuronal responses in the MST, DLPN, and VPFL represent information on retinal errors under a single or narrow stimulus range. Additionally, in the eye-movement model, the differences between the distributions of CDs under local and global fitting (*right*) were also significant for the MST and DLPN neurons, ($P = 0.0001$ and $P = 0.0014$, respectively). However, as shown in Fig. 10*F*, this difference was not significant for VPFL P-cells ($P = 0.15$), and their firing patterns were frequently reconstructed well from eye movements. These results indicate that only neuronal responses in the VPFL represented motor command information independent of the stimulus conditions.

By comparing performances in the retinal error model and eye-movement model under local fitting, the features of MST and DLPN neurons become clearer. Under local fitting, the differences between the CD distributions in the retinal error and eye-movement models were significant ($P < 0.0001$) for both the MST and DLPN neurons (*left boxes* in *A* vs. *B* and *C* vs. *D*). On the other hand, this difference was not significant ($P = 0.14$) for the VPFL P-cells (*left boxes* in *E* vs. *F*). These results indicate that the retinal error model describes the temporal firing patterns of the MST and DLPN neurons more accurately than the eye movement model. These results also indicate that the firing patterns of VPFL P-cells were well reconstructed both from retinal errors and from eye movements under local fitting.

On the other hand, by comparing the performances in the retinal error and eye-movement models under global fitting, the features of P-cells become clearer. Under global fitting, the fitting performances in the eye-movement model were better than those in the retinal error model for the MST, DLPN, and VPFL (these differences were significant at $P < 0.002$, $P < 0.04$, and $P = 0.0002$, respectively), although the performance of the eye-movement model for most MST and DLPN neurons was still insufficient. As described in the preceding text, sufficient performance by the eye-movement model under global fitting was only obtained for the P-cells in the VPFL.

DISCUSSION

Description of the relationship between sensory/motor information and neuronal activity

As shown in the preceding analyses, we quantified the relationship among the temporal firing patterns for single neurons in the MST, DLPN, and VPFL and eye movements or retinal errors. The advantage of this method is that by applying both local and global linear regression analyses, we can both argue the global linearity and global characteristics of the cell firing and examine the local representation of the cell firing within a limited stimulus range. The ability to perform linear-regression analyses and compare the estimated coefficients obtained by local and global analyses for the three regions (MST, DLPN, and VPFL) has made it possible for us to consider signal transformation in the process of eye motor command generation.

Instead of taking the "piecewise linear" analysis approach, one could try to consider nonlinearities concealed in the relationships between sensory/motor information and neuronal firing patterns. Previous studies (Kawano et al. 1992, 1994) and our preliminary analysis suggest that three nonlinear factors should be considered in characterizing the "global" MST and DLPN activities and speed preference in each neuron. First, even in a particular neuron, the neuronal response latencies differ according to stimulus speed. Second, the sensitivity of the acceleration and velocity components varies according to the stimulus speed. Third, there is a difference between the sensitivity changes of the acceleration and velocity components according to stimulus speed. To consider all of these nonlinear factors for global fitting, however, we need to use a complicated nonlinear model, which may be hardly justified and does not give any clear view without sufficient data analysis to characterize these nonlinear factors. Further experiments using various visual stimuli having complex profiles are needed to capture the nonlinearities between retinal errors and neural responses under the global condition.

Another interesting point is the effect of eye movement on the neuronal activities in each region. Several studies have reported continuous neuronal activities in the MST (Bradley et al. 1996; Newsome et al. 1988; Sakata et al. 1983; Squatrito and Maioli 1996), DLPN (Mustari et al. 1988; Suzuki and Keller 1984; Thier et al. 1988), and VPFL (Lisberger and Fuchs 1978a,b; Miles and Fuller 1975) without a visual target during smooth pursuit eye movements. Previous studies of the ocular following response, however, have demonstrated that the discharges of MST and DLPN neurons and P-cells increase before eye movement (Gomi et al. 1998; Kawano and Shidara 1993; Kawano et al. 1992, 1994; Shidara and Kawano 1993; Shidara et al. 1993) and abruptly decay when the moving visual scene is blanked (Gomi et al. 1998; Kawano et al. 1992). Thus the closed-loop portion of the temporal firing patterns during the ocular following responses in this study need not be considered an effect of eye movement on neuronal activity (extra-retinal information).

Information represented in the neuronal activities of the MST and DLPN

In the analyses shown in the preceding text, several common characteristics can be found in the firing patterns of MST and DLPN neurons. First, the temporal firing patterns were accurately described by the models under local rather than global fitting. In addition, under local fitting, the temporal firing patterns of the MST and DLPN neurons were modeled better by retinal errors than by eye movements. These results suggest that the temporal pattern of each neuron in the MST and DLPN represents retinal error information within the limited stimulus range. Second, under local fitting using the retinal error model, the acceleration and velocity coefficients of the MST and DLPN were broadly distributed, whereas those of the VPFL were more compact (Fig. 4). This suggests that the MST and DLPN neurons encode a variety of dynamic visual properties and that some are dominated by the acceleration component, some are dominated by the velocity component, and others are indifferent. Furthermore, the acceleration component of retinal errors contributed more significantly to the temporal firing

patterns of MST and DLPN neurons than it did for P-cells. From these results, it may be inferred that information on retinal errors is integrated to represent the appropriate temporal firing patterns of P-cells to drive eye movements.

As for the similarity in the neuronal responses of the MST and DLPN neurons, it has been reported (Kawano et al. 1992, 1994) that there are no significant differences in directional preference (ipsiversive/contraversive or up/down) in these regions. It has also been reported that most direction-selective neurons show their strongest responses at high stimulus speeds, but the remainder show their strongest responses at low stimulus speeds. In the present study, we observed a significant difference in preferred speeds between the MST and DLPN. Furthermore, in the MST, the best CD was related to "preferred speed." Thus when a neuron preferred faster speeds, its CD tended to be higher at faster speeds, and when a neuron preferred slower speeds, its CD tended to be higher at slower speeds. These results suggest that the temporal patterns of MST neurons represent information on retinal errors around the preferred stimulus. Previous reports have shown that there is a wide range of receptive field sizes in the MST, whereas DLPN neurons have large receptive fields (Suzuki et al. 1990; Thier et al. 1988). These studies suggested that there is spatial integration of information from the MST to the DLPN. Even so, in this study, no clear difference was observed between MST and DLPN neurons in temporal firing patterns. It is possible that information on retinal errors may be integrated spatially (i.e., receptive field and preferred speed) rather than temporally from the MST to the DLPN.

A recent study on disparity-induced vergence eye movements suggests that the discharges of individual MST neurons encode some limited aspect(s) of the stimulus disparity and/or the vergence motor response, whereas the summed activity of the population encodes the entire vergence velocity response (Takemura et al. 2001). In this study, to see how well the discharges of the entire population of MST or DLPN neurons encoded the motor command for the ocular following responses, we had to analyze the temporal firing patterns of neurons in response to a given direction and speed in the same monkey, regardless of the preferred stimulus of the neurons. Since we only have data on the response to the preferred stimulus for each cell in this study, we are unable to determine whether the neuronal population average represents the motor command for the ocular following response.

Information represented in the activities of the VPFL P-cells

Our results show that the temporal firing patterns of VPFL P-cells can be described by the eye-movement model under global fitting, suggesting that P-cells have the appropriate global characteristics for motor command. Previous studies have shown that VPFL P-cells have different response properties than MST and DLPN neurons to visual stimuli like those in the ocular following response (Kawano et al. 1996). First, the distribution of their preferred directions during the ocular following response has clearly divided the VPFL P-cells into two classes: horizontal P-cells, which preferred ipsiversive movement, and vertical P-cells, which preferred downward movement. Second, P-cells showed their best responses at high stimulus speeds. Most MST and DLPN neurons also showed their best responses at high stimulus speeds, although some neurons preferred lower stimulus speeds. These results indicate that P-cells increase their discharge rate in response to a wide range of stimulus speeds and do so in proportion to the stimulus speed. Third, a linear relationship between neuronal firing patterns and eye movements was observed. This study demonstrated that P-cells already encode the dynamic component of the motor command for ocular following. They do so under multiple stimulus conditions, which agrees with the observations of previous studies.

As for the positional component of eye movements, it has been reported that VPFL P-cell activities show a weakly positive correlation or no correlation with eye position (Krauzlis 2000; Krauzlis and Lisberger 1994; Miles et al. 1980). In this study, VPFL P-cell activities during ocular following negatively correlated with eye position. Furthermore, the magnitudes of these correlations were not negligible. Gomi et al. (1998) have already discussed in detail how the position components have a reversed sign relative to eye movements. Additionally, Kitama et al. (1999) used the acceleration, velocity, and position of eye movements in cats to analyze the temporal firing patterns of simple spikes from P-cells during optokinetic response (OKR). When they controlled the initial eye position to examine the contribution of eye position to the firing pattern, the absolute eye position was not encoded in the temporal firing pattern during OKR. Furthermore, we attempted to determine whether these discrepant findings might have been caused by the omission of the slide component, which shows the time decay component of the firing rate (Krauzlis 2000). To explain the time decay of P-cell firing, *Eq. 3* was used. *Equation 3* is equivalent to the model proposed by Goldstein and Robinson (1986) and Optican and Miles (1985) and can be written as

$$\hat{f}(t-\delta) = a \cdot \ddot{x}(t) + b \cdot \dot{x}(t) + c \cdot x(t) + d - \mathrm{Ts} \cdot \dot{\hat{f}}(t-\delta) \qquad (3)$$

where $\hat{f}(t)$, $\dot{\hat{f}}(t)$, $\ddot{x}(t)$, $\dot{x}(t)$, $x(t)$, and δ are the reconstructed firing frequency of a neuron; the time derivative of the firing rate; the acceleration, velocity, and position of eye movements at time *t;* and the time delay, respectively. Five coefficients (*a*, *b*, *c*, *d*, and Ts) and the time delay (δ) were estimated in such a way as to minimize the squared estimation error. The result of the calculation was that the coefficients of the positional component were still large negative values. Therefore the slide component in P-cell firing [$\dot{\hat{f}}(t)$] in *Eq. 3* does not explain the negative correlation with eye position in our results.

In the retinal error model, the temporal firing patterns of VPFL P-cells were not described under global fitting. Under local fitting, the firing of P-cells fitted better than that of MST and DLPN neurons under local fitting (Fig. 9, *A, C,* and *E, left*). These results can be explained as follows: P-cells receive the visual information from the DLPN and MST, and DLPN and MST neurons have a narrow range of preferred stimulus speeds, so their temporal firing patterns encode the local representation of retinal errors. Since the local visual information converges on a P-cell, the temporal firing patterns do not relate to retinal errors globally. On the other hand, the temporal firing patterns at every stimulus speed relate to retinal errors locally.

Transformation of visual input into eye motor commands

In this study, we were unable to determine whether the neurons we observed in the MST and DLPN send signals to the

next stage of information processing. These neurons could just function as local interneurons or could project to regions unrelated to ocular-following eye movements. However, neurons in the DLPN, which is the next stage after the MST, share many characteristics with neurons in the MST (Figs. 4 and 8). This suggests that there is little possibility that only MST neurons that fitted well with eye movements project to the DLPN. Furthermore, it has also been reported that the visual response properties of visual mossy fibers in the VPFL are similar to those of DLPN and MST neurons (Kawano and Shidara 1993; Shidara et al. 1993). The temporal firing patterns of visual mossy fibers were also similar to those of DLPN and MST neurons and were modeled from eye movements under local fitting but not under global fitting (unpublished data). This suggests that the neuronal signals observed in the DLPN project as the inputs to the VPFL; therefore it is unlikely that only well-fitted neurons in the DLPN project to the VPFL.

Glickstein et al. (1994) reported that there is a sparse but definite projection to the VPFL but that the major visual pontine projection is to the dorsal rather than ventral paraflocculus. To study the role of the dorsal paraflocculus during the ocular following responses, single-unit recording and quantitative analysis are required. Although, evidence from focal chemical lesions of the MST, DLPN, and VPFL suggests that the MST, DLPN, and VPFL play a role in the early phase of the ocular following response. The temporal firing pattern characteristics observed in this study and the visual properties found in previous studies support the following ideas. *1*) Single cells in the MST encode limited visual information extracted by the visual cortex in their temporal firing patterns. They do so only when a visual stimulus is given in the receptive field with the preferred direction and speed. *2*) Single cells in the DLPN receive spatially integrated visual information (e.g., receptive field, preferred speed) from MST neurons. Here the temporal firing patterns in the MST and DLPN do not yet represent the dynamic component of the motor command. Rather they represent the dynamic properties of the visual stimulus in a limited range by various combinations of the acceleration, velocity, and position components of retinal errors. MST and DLPN neurons vary somewhat in their properties. However, as a whole, they encode the dominant acceleration component that is probably integrated prior to the VPFL P-cells' firing patterns. And *3*) single P-cells receive spatially and temporally integrated visual information (e.g., preferred direction) from DLPN neurons, mediated by visual mossy fibers. The temporal firing pattern of P-cells analyzed in this study was the simple spike, which results from the synaptic action of granule cell axon terminals. The granule cells receive mossy fiber inputs from the brain stem and send axons up to the molecular layer, where they bifurcate and traverse as parallel fibers, making numerous serial contacts with P-cell dendrites. In this study, it is conceivable that the retinal error information encoded in the temporal patterns of DLPN neurons converges on a P-cell in the VPFL. Thus a potential explanation is that every single P-cell receives a large number of inputs with various time delays, and these inputs are summed together into the temporal firing pattern of a P-cell. Therefore the temporal firing patterns of the P-cells represent temporally integrated visual information. At the same time, the P-cells' firing represents the dynamic motor command independent of the stimulus speed. We conclude that sensory-to-motor transformation for ocular following occurs at the P-cell.

APPENDIX

Modeling check (Cp statistics)

To find the model that best represented the observed firing patterns, we examined several models that had combinations of acceleration, velocity, and position terms with bias and delay. The best model was evaluated using Cp statistics, which test whether the increased parameter can be traded for the goodness of model fit (Gomi et al. 1998; Hines and Montgomery 1972). The equation used for finding the Cp-statistics value was as follows

$$\mathrm{Cp} = \frac{\sum_t (\hat{f}(t) - f(t))^2}{\sigma^2} - n + 2p \tag{A1}$$

where n is the number of data points for the regression, p is the number of degrees of freedom for the model, σ^2 is the estimated population variance, $\hat{f}(t)$ is the reconstructed firing frequency, and $f(t)$ is the observed firing frequency. In this analysis, we used the estimated variance of the full-term model (*Eq. 1*) as the estimated population variance, σ^2. By selecting a model having the minimum Cp statistics, it is possible to find the best model taking into account the tradeoff between the model size and fitting error.

Representation of retinal error model

We analyzed the temporal firing patterns using the retinal error model in *Eq. 1*. It is possible, however, that another model with fewer parameters may be sufficient for fitting the temporal firing patterns. In other words, one of the parameters in *Eq. 1* might be unnecessary to accurately represent temporal firing patterns. For this reason, we examined all models that combined acceleration, velocity, and position terms with bias and delay

$$\hat{f}(t - \delta) = a \cdot \ddot{x}(t) + b \cdot \dot{x}(t) + c \tag{A2}$$

$$\hat{f}(t - \delta) = a \cdot \ddot{x}(t) + b \cdot x(t) + c \tag{A3}$$

$$\hat{f}(t - \delta) = a \cdot \dot{x}(t) + b \cdot x(t) + c \tag{A4}$$

$$\hat{f}(t - \delta) = a \cdot \ddot{x}(t) + b \tag{A5}$$

$$\hat{f}(t - \delta) = a \cdot \dot{x}(t) + b \tag{A6}$$

$$\hat{f}(t - \delta) = a \cdot x(t) + b \tag{A7}$$

In most of the MST and DLPN neuron datasets, the Cp-statistics' values were lowest for *Eq. 1* in the retinal error model under local fitting (62.6%, 82/131 and 61.4%, 70/114, respectively). On the other hand, in 65/89 (73.0%) of the VPFL P-cell datasets, the model for velocity and position of retinal errors performed best (7). These results are consistent with those of the *t*-test (Table 1*A*) and suggest that the acceleration component of retinal errors contributed more significantly to the temporal firing patterns in the MST and DLPN regions than it did to P-cell firing in the VPFL.

Representation of eye-movement model

In local fitting, the Cp-statistics' value was lowest for *Eq. 1* among all of the models we tested in most of the datasets: 75.8% (75/99) for the MST, 81.8% (72/88) for the DLPN, and 90.4% (75/83) for the VPFL. Additionally, in global fitting, for all the neurons except one P-cell (11/11 in the MST, 10/10 in the DLPN, and 16/17 P-cells), the Cp-statistics value was lowest for *Eq. 1*. These results indicate that all of the components of eye movements in *Eq. 1* are required to represent

the temporal firing patterns. Therefore the model in *Eq. 1* was the best among those we tested, in both local and global fitting.

We are grateful to Dr. F. A. Miles for comments while preparing the manuscript. We thank Drs. M. Shidara, Y. Kodaka, and K. Miura for valuable advice and Dr. S. Yamane for continuing encouragement. We also thank M. Okui-Uchiyama, A. Kameyama, and T. Takasu for technical assistance and Y. Yaguchi and S. Inoue for secretarial assistance.

REFERENCES

BRADLEY DC, MAXWELL M, ANDERSEN RA, BANKS MS, AND SHENOY KV. Mechanisms of heading perception in primate visual cortex. *Science* 273: 1544–1547, 1996.

BRODAL P. The corticopontine projection in the rhesus monkey. Origin and principles of organization. *Brain* 101: 251–283, 1978.

BRODAL P. The pontocerebellar projection in the rhesus monkey: an experimental study with retrograde axonal transport of horseradish peroxidase. *Neuroscience* 4: 193–208, 1979.

BRODAL P. Further observations on the cerebellar projections from the pontine nuclei and the nucleus reticularis tegmenti pontis in the rhesus monkey. *J Comp Neurol* 204: 44–55, 1982.

CRIST CF, YAMASAKI DS, KOMATSU H, AND WURTZ RH. A grid system and a microsyringe for single cell recording. *J Neurosci Methods* 26: 117–122, 1988.

FUCHS AF AND ROBINSON DA. A method for measuring horizontal and vertical eye movement chronically in the monkey. *J Appl Physiol* 21: 1068–1070, 1966.

GLICKSTEIN M, COHEN JL, DIXON B, GIBSON A, HOLLINS M, LABOSSIERE E, AND ROBINSON F. Corticopontine visual projections in macaque monkeys. *J Comp Neurol* 190: 209–229, 1980.

GLICKSTEIN M, GERRITS N, KRALJ-HANS I, MERCIER B, STEIN J, AND VOOGD J. Visual pontocerebellar projections in the macaque. *J Comp Neurol* 349: 51–72, 1994.

GLICKSTEIN M, MAY JG, AND MERCIER BE. Corticopontine projection in the macaque: the distribution of labelled cortical cells after large injections of horseradish peroxidase in the pontine nuclei. *J Comp Neurol* 235: 343–359, 1985.

GOLDSTEIN HP AND ROBINSON DA. Hysteresis and slow drift in abducens unit activity. *J Neurophysiol* 55: 1044–1056, 1986.

GOMI H, SHIDARA M, TAKEMURA A, INOUE Y, KAWANO K, AND KAWATO M. Temporal firing patterns of Purkinje cells in the cerebellar ventral paraflocculus during ocular following responses in monkeys. I. Simple spikes. *J Neurophysiol* 80: 818–831, 1998.

HINES WW AND MONTGOMERY DC. *Probability and Statistics in Engineering and Management Science* (3rd ed.). New York: Wiley, 1972.

JUDGE SJ, RICHMOND BJ, AND CHU FC. Implantation of magnetic search coils for measurement of eye position: an improved method. *Vision Res* 20: 535–538, 1980.

KAWANO K AND MILES FA. Short-latency ocular following responses of monkey. II. Dependence on a prior saccadic eye movement. *J Neurophysiol* 56: 1355–1380, 1986.

KAWANO K AND SHIDARA M. The role of the ventral paraflicculus in ocular following in the monkey. In: *Role of the Cerebellum and Basal Ganglia in Voluntary Movement.* Amsterdam: Elsevier Science, 1993, p. 195–202.

KAWANO K, SHIDARA M, WATANABE Y, AND YAMANE S. Neural activity in cortical area MST of alert monkey during ocular following responses. *J Neurophysiol* 71: 2305–2324, 1994.

KAWANO K, SHIDARA M, AND YAMANE S. Relation of the dorsolateral pontine nucleus of the monkey to ocular following responses. *Soc Neurosci Abstr* 16: 902, 1990.

KAWANO K, SHIDARA M, AND YAMANE S. Neural activity in dorsolateral pontine nucleus of alert monkey during ocular following responses. *J Neurophysiol* 67: 680–703, 1992.

KAWANO K, TAKEMURA A, INOUE Y, KITAMA T, KOBAYASHI Y, AND MUSTARI MJ. Visual inputs to cerebellar ventral paraflocculus during ocular following responses. *Prog Brain Res* 112: 415–422, 1996.

KELLER EL. Accommodative vergence in the alert monkey. Motor unit analysis. *Vision Res* 13: 1565–1575, 1973.

KITAMA T, OMATA T, MIZUKOSHI A, UENO T, AND SATO Y. Motor dynamics encoding in cat cerebellar flocculus middle zone during optokinetic eye movements. *J Neurophysiol* 82: 2235–2248, 1999.

KRAUZLIS RJ. Population coding of movement dynamics by cerebellar Purkinje cells. *Neuroreport* 11: 1045–1050, 2000.

KRAUZLIS RJ AND LISBERGER SG. Simple spike responses of gaze velocity Purkinje cells in the floccular lobe of the monkey during the onset and offset of pursuit eye movements. *J Neurophysiol* 72: 2045–2050, 1994.

LANGER T, FUCHS AF, SCUDDER CA, AND CHUBB MC. Afferents to the flocculus of the cerebellum in the rhesus macaque as revealed by retrograde transport of horseradish peroxidase. *J Comp Neurol* 235: 1–25, 1985.

LISBERGER SG AND FUCHS AF. Role of primate flocculus during rapid behavioral modification of vestibuloocular reflex. I. Purkinje cell activity during visually guided horizontal smooth-pursuit eye movements and passive head rotation. *J Neurophysiol* 41: 733–763, 1978a.

LISBERGER SG AND FUCHS AF. Role of primate flocculus during rapid behavioral modification of vestibuloocular reflex. II. Mossy fiber firing patterns during horizontal head rotation and eye movement. *J Neurophysiol* 41: 764–777, 1978b.

MAUNSELL JH AND VAN ESSEN DC. The connections of the middle temporal visual area (MT) and their relationship to a cortical hierarchy in the macaque monkey. *J Neurosci* 3: 2563–2586, 1983.

MAY JG AND ANDERSEN RA. Different patterns of corticopontine projections from separate cortical fields within the inferior parietal lobule and dorsal prelunate gyrus of the macaque. *Exp Brain Res* 63: 265–278, 1986.

MILES FA AND FULLER JH. Visual tracking and the primate flocculus. *Science* 189: 1000–1002, 1975.

MILES FA, FULLER JH, BRAITMAN DJ, AND DOW BM. Long-term adaptive changes in primate vestibuloocular reflex. III. Electrophysiological observations in flocculus of normal monkeys. *J Neurophysiol* 43: 1437–1476, 1980.

MILES FA AND KAWANO K. Short-latency ocular following responses of monkey. III. Plasticity. *J Neurophysiol* 56: 1381–1396, 1986.

MILES FA, KAWANO K, AND OPTICAN LM. Short-latency ocular following responses of monkey. I. Dependence on temporospatial properties of visual input. *J Neurophysiol* 56: 1321–1354, 1986.

MUSTARI MJ, FUCHS AF, AND WALLMAN J. Response properties of dorsolateral pontine units during smooth pursuit in the rhesus macaque. *J Neurophysiol* 60: 664–686, 1988.

NAGAO S, KITAMURA T, NAKAMURA N, HIRAMATSU T, AND YAMADA J. Differences of the primate flocculus and ventral paraflocculus in the mossy and climbing fiber input organization. *J Comp Neurol* 382: 480–498, 1997.

NEWSOME WT, WURTZ RH, AND KOMATSU H. Relation of cortical areas MT and MST to pursuit eye movements. II. Differentiation of retinal from extraretinal inputs. *J Neurophysiol* 60: 604–620, 1988.

OPTICAN LM AND MILES FA. Visually induced adaptive changes in primate saccadic oculomotor control signals. *J Neurophysiol* 54: 940–958, 1985.

SAKATA H, SHIBUTANI H, AND KAWANO K. Functional properties of visual tracking neurons in posterior parietal association cortex of the monkey. *J Neurophysiol* 49: 1364–1380, 1983.

SHIDARA M AND KAWANO K. Role of Purkinje cells in the ventral paraflocculus in short-latency ocular following responses. *Exp Brain Res* 93: 185–195, 1993.

SHIDARA M, KAWANO K, GOMI H, AND KAWATO M. Inverse-dynamics model eye movement control by Purkinje cells in the cerebellum. *Nature* 365: 50–52, 1993.

SHIDARA M, KAWANO K, AND YAMANE S. Ocular following response deficits with chemical lesions in the medial superior temporal area of the monkey. *Neurosci Res* 14: 1991.

SQUATRITO S AND MAIOLI MG. Gaze field properties of eye position neurones in areas MST and 7a of the macaque monkey. *Vis Neurosci* 13: 385–398, 1996.

SUZUKI DA AND KELLER EL. Visual signals in the dorsolateral pontine nucleus of the alert monkey: their relationship to smooth-pursuit eye movements. *Exp Brain Res* 53: 473–478, 1984.

SUZUKI DA, MAY JG, KELLER EL, AND YEE RD. Visual motion response properties of neurons in dorsolateral pontine nucleus of alert monkey. *J Neurophysiol* 63: 37–59, 1990.

TAKEMURA A, INOUE Y, GOMI H, KAWATO M, AND KAWANO K. Analysis of neuronal activities during ocular following responses in alert monkeys. In: *Technical Report of IEICE. NC99-22.* 1999, p. 77–84.

TAKEMURA A, INOUE Y, GOMI H, KAWATO M, SHIDARA M, AND KAWANO K. Analysis of neural activity during ocular following. In: *Proceedings of SICE. The 11th Symposium Biological and Physiological Engineering.* 1996, p. 305–308.

TAKEMURA A, INOUE Y, AND KAWANO K. The role of MST neurons in short-latency visual tracking eye movements. *Soc Neurosci Abstr* 26: 1715, 2000.

TAKEMURA A, INOUE Y, KAWANO K, QUAIA C, AND MILES FA. Single-unit activity in cortical area MST associated with short-latency disparity-vergence eye movements: evidence for population coding. *J Neurophysiol* 85: 2245–2266, 2001.

THIER P, KOEHLER W, AND BÜETTNER UW. Neuronal activity in the dorsolateral pontine nucleus of the alert monkey modulated by visual stimuli and eye movements. *Exp Brain Res* 70: 496–512, 1988.

UNGERLEIDER LG, DESIMONE R, GALKIN TW, AND MISHKIN M. Subcortical projections of area MT in the macaque. *J Comp Neurol* 223: 368–386, 1984.

WURTZ RH. Visual receptive fields of striate cortex neurons in awake monkeys. *J Neurophysiol* 32: 727–742, 1969.